Elastic Element Integration for Improved Flapping-Wing Micro Air Vehicle Performance

Ranjana Sahai, Kevin C. Galloway, and Robert J. Wood, *Member, IEEE*

***Abstract*—This paper studies flapping-wing micro air vehicles (FWMAV) whose transmission mechanisms use flexures as energy storage elements to reduce needed input power. A distinguishing feature of the proposed four-bar mechanism is the use of rubber-based flexures in two of its joints. These lightweight and compact flexures have been used for the first time in the design of an FWMAV whose projected total weight is approximately 3 g. This paper discusses in detail how the flexures were designed and how the challenges associated with their fabrication were met. Flexure stiffnesses were chosen based upon a simple, computationally efficient model of the four-bar mechanism actuated by an electric motor to flap two wings at 18 Hz. An instrumented test stand was designed to easily replace the upper part of the four-bar flexure mechanism and wings, and it was used to experimentally determine the power savings associated with flexures of different stiffnesses. While the measured power savings (maximum of 20%) may seem modest, they were nevertheless significant, considering that the use of the rubber-based flexures produced approximately 0.3 g added thrust at a less than 1% cost in weight (0.02 g).**

***Index Terms*—Biologically inspired robots, flapping wing, mechanism design, microrobots.**

I. Introduction

In nature, animals of all sizes exploit elastic mechanisms for a variety of purposes. These uses range from shock absorbers in footpads, to catapult aids for jumping, to energy storage return for running, swimming, and flying [1]. Scientists have increasingly recognized the advantages of employing elastic elements in robotics as well. In the development of biomimetic walking robots, Pratt and Williamson [2] discovered that the introduction of a spring in series between the motor's gear train and load results in a system that is inherently tolerant to shock or unexpected collisions. Additional advantages include low impedance and improved force control stability [3]. The use of elastic spring elements also features heavily in the design of jumping robots. Both Kovac *et al.* [4] and Scarfogliero *et al.* [5] store potential energy for their 5-cm robots, weighing 7 and 15 g, respectively, in traditional torsional and linear springs. In their development of a 10-mg, millimeter-sized, jumping robot, Churaman *et al.* have proposed a version with silicone rubber (polydimethylsiloxane: PDMS) features incorporated in silicon structures. Here, the deflection of the PDMS elements serves as a means for the jump energy storage [6].

While the inclusion of spring elements in jumping robots is almost universal, their use in robotic flyers is not as prevalent, particularly in flapping-wing systems powered with conventional motors. Flapping-wing micro air vehicles (FWMAV) typically consist of an actuator coupled to the wings through an articulated transmission. When the chosen actuator is a DC motor, the logical place to incorporate elasticity is in the transmission. Considering this, a theoretical study by Khatait *et al.* revealed that the introduction of discrete compliant components in a typical four-bar transmission of a FWMAV yields a reduction in the peaks of the driving torque by a factor of 2.85. In their case, the discrete compliant components were two flexural pivots that replaced two out of the four pin joints [7]. Similarly, Tantanawat and Kota conducted a study looking at the minimization of peak input power by utilizing the energy return of a fully compliant transmission mechanism. They argued that the use of a fully compliant mechanism could require 48% less peak power than its rigid counterpart and 10% less than a system with a discrete spring [8]. Neither case, however, is supplemented with experimental evidence. In practice, a few groups have implemented springs or elastic elements in their design of flying mechanisms. Baek *et al.* analyze a mass–spring system coupled to a motor-driven slider crank mechanism to show that the addition of a linear spring to two kinds of transmission systems can potentially yield up to a 30% power reduction in one case and 19% reduction in the other [9]. The Agrawal group has also demonstrated the use of springs in flying prototypes. In [10], they added two linear springs to store and release energy during the wing upstroke and downstroke. In [11], they developed a prototype with added elastic bands in the transmission for flapping stiffness and a rod at the wing root for stiffness during wing rotation. A separate group looked at utilizing a fully compliant frame as the elastic element [12].

In all these previous works, however, even if a theoretically motivated optimum spring stiffness is derived, no systematic methodology for incorporating this spring stiffness into the structure is given beyond using traditionally rated metal wire springs. Since weight and compactness are of primary importance for FWMAVs, the use of other materials warrants consideration. In addition, most of the experimental data are limited to two distinct cases: spring or no spring. Since even very detailed

Manuscript received February 13, 2012; revised August 24, 2012; accepted September 5, 2012. Date of publication October 9, 2012; date of current version February 1, 2013. This paper was recommended for publication by Associate Editor Y. Sun and Editor B. J. Nelson upon evaluation of the reviewers' comments. This work was supported in part by the Air Force Office of Scientific Research under Award #FA9550-10-C-0044 under a subcontract from Physical Sciences Inc.

The authors are with the Harvard Microrobotics Laboratory, Harvard University, Cambridge, MA 02138 USA, and also with the Wyss Institute for Biologically Inspired Engineering, Harvard University, Boston, MA 02115 USA (e-mail: rsahai@seas.harvard.edu; kevin.galloway@wyss.harvard.edu; rjwood@seas.harvard.edu.).

Color versions of one or more of the figures in this paper are available online at http://ieeexplore.ieee.org.

Digital Object Identifier 10.1109/TRO.2012.2218936

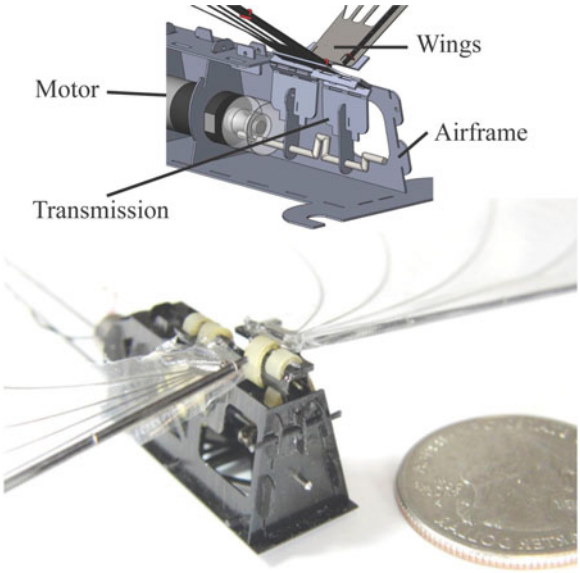

Fig. 1. FWMAV and a CAD model showing a cutaway of the inside main drivetrain.

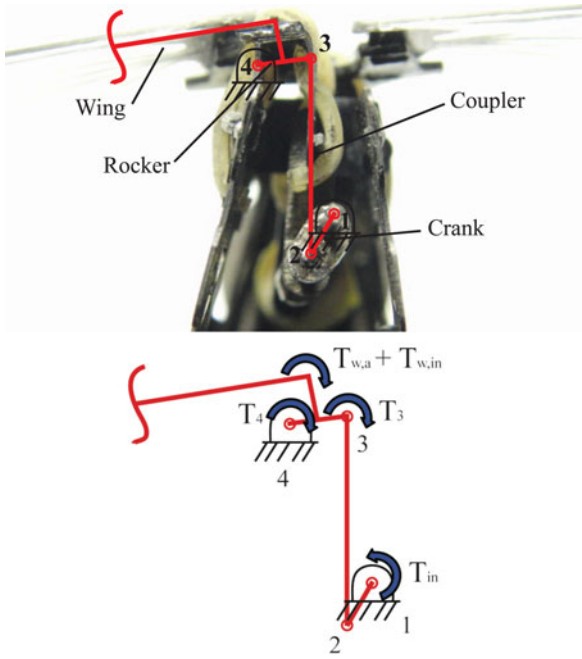

Fig. 2. (Top) FWMAV's transmission forming a four-bar. (Bottom) Resulting free body diagram of the four-bar transmission with the various torques taken into account in the dynamic analysis of the mechanism.

theoretical analyses cannot hope to capture all the interactions in these systems, seeing experimental trends of varying stiffness can be beneficial. In what follows, we begin by describing an analysis of a typical transmission and show the impact of joint stiffness on the required input torque. Using an optimized stiffness extracted from this analysis, we then design flexure joints with the appropriate revolute stiffness. Material considerations are discussed along with the resulting fabrication issues. We then use our custom developed FWMAV system where the main components can be interchanged to vary the stiffness while measuring power, frequency, and thrust. The results are then presented and discussed.

II. Theoretical Motivation

A. Basic System Description

The main drivetrain of a typical FWMAV consists of a primary actuator, wings, and an intermediate transmission mechanism that converts actuator motion into the flapping motion of the wings. Fig. 1 shows a cutaway displaying this drivetrain of the FWMAV. For the experimental device constructed here, we have used commercially available DC motors as the primary actuators and a four-bar transmission mechanism, as was done in many of the FWMAVs that have successfully flown at this size scale. In addition, we have employed compliant structures as lumped elements in the form of flexures rather than using a fully compliant structure. Using a combination of flexures and rigid elements leads to a much more simplified analysis than that required for fully compliant structures, and getting away from traditional springs allows the use of material and shapes that can be easily incorporated into the current fabrication techniques (see Section III-B), leading to more robust and compact structures. In addition to high computational cost in modeling, fully compliant structures would also require custom fabrication each time the stiffness needs to be altered.

The mechanism (see Fig. 1) we will consider here is thus a hybrid combination of pins, flexures, and rigid elements. Flexures provide a lightweight and compact means of storing energy that may potentially lead to significant savings in power requirements, as shown in the following analysis. We will outline our analysis to determine the tuned flexure stiffnesses using a four-bar transmission. However, the procedure described in the following can be similarly applied to other types of transmission as well.

B. Analysis Procedure

The analysis to determine an optimal flexure stiffness to minimize input torque requires solving the kinematic and dynamic equations of the system. For purposes of reference, we name the joints between the crank and ground link sequentially 1–4, as shown in Fig. 2. Because of practical considerations in the four-bar transmission fabrication, only joints 3 and 4 are flexure joints (joint 1 is the gear axle and joint 2 is a pin joint; see Fig. 1). In order to keep the analysis simple, we have made several key assumptions outlined in the following that capture the essential physics of the problem and yet reduce the computational costs significantly.

1) As is often done, we will assume that the kinematic analysis can be decoupled from the dynamic analysis. This allows us to carry out the kinematic analysis first using the well-known standard procedures for a four-bar mechanism by further assuming all four joints to be pin joints. This analysis provides the needed information about velocity and acceleration for the dynamic analysis.
2) For the dynamic analysis, we will assume that the flapping motion of the wing can be decoupled from its rotational

(i.e., "feathering") motion. In terms of the coordinate system used here, the coupling term is multiplied by the difference in moment of inertias ($I_{yy} - I_{zz}$) (see, for example, [13]) which is very small for the wings utilized in our experimental work. (For our wings, I_{yy} is 141 g $\cdot$ mm^2, and I_{zz} is 153 g $\cdot$ mm^2; hence, their difference is only 12 g $\cdot$ mm^2.) The assumed decoupling is, therefore, justified, and we will solely consider flapping motion in this study.

3) We will further consider the light-weight carbon fiber links to essentially have no mass. However, in order to take their mass partially into account, we will, using the concept of lumped analysis, divide the total mass of the links between the crank and the wing. This assumption allows us to consider the inertial terms only for the crank and the wings, which only undergo a purely circular motion about a fixed axis.
4) In addition, we will characterize the flexures by the well-known quasi-static pseudorigid body model [14], the procedure for which is described later in this section. Finally, the aerodynamic torques will be represented by the quasi-steady blade element analysis [15].
5) The apparent mass effect will be included in the present analysis. This mass represents the air that is accelerated by the wing and is estimated as the mass of air contained in a cylinder whose diameter is equal to the wing chord c and whose length is equal to the wing span L [16]. The apparent mass is thus equal to $\rho(\frac{\pi c^2}{4})L$ and is simply added to the wing mass. The apparent mass effect is significant in small vehicles with relatively large wings (as is the case here), especially in hover.

We will first use the D'Alembert's principle to convert the dynamics problem to an equivalent statics problem. This requires adding inertial terms that, for circular motion, are forces of magnitude $mr\omega^2$ and $mr\alpha$ and a torque equal to $I\alpha$. Here, I represents the mass moment of inertia about a center of mass axis parallel to the axis about which the wing flaps, r is the distance of the center of mass from the axis of rotation, and ω and α are, respectively, the angular velocity and angular acceleration. The first force ($mr\omega^2$) does not contribute to the torque since its line of action passes through the fixed axis of rotation.

It will be convenient to use the power analysis method described in [17] since it eliminates the need for determining the joint reaction forces. For a preliminary analysis, we will assume that the motor runs at steady state ($\alpha_{\text{crank}} = 0$) so that there is no inertial contribution for the crank. Assuming a rectangular wing (with length L chosen so that its mass moment of inertia is equal to that of the fabricated wing as determined by its SolidWorks model), the total inertial contribution to power for the wing is simply given by total inertial torque $T_{w,i}$ times the angular velocity ω_w, or

$$T_{w,i}\omega_w = \frac{1}{3}mL^2\alpha_w\omega_w. \tag{1}$$

Here, L is the wing length, and $\frac{1}{3}mL^2$ is the inertia of the wing. The contribution to the power due to aerodynamic damping is the damping torque $T_{w,a}$ multiplied by the angular velocity ω_w. Based on the blade element theory [15], the damping torque $T_{w,a}$ can be described in terms of the drag coefficient C_D as

$$T_{w,a} = \frac{1}{2}\rho C_D \int_0^L r(r\omega_w)^2 \text{sgn}(\omega_w)c(r)dr. \tag{2}$$

Here, ρ is the air density. This expression can be rewritten in terms of a damping coefficient B_0 as follows:

$$T_{w,a} = B_0\omega_w^2 \text{sgn}(\omega_w). \tag{3}$$

Since we are approximating the wing as an equivalent rectangular shape with length L and width c (where c is the average chord length determined by wing surface area equivalence), B_0 becomes

$$B_0 = \frac{1}{8}\rho C_D L^4 c. \tag{4}$$

Using the well-known pseudorigid body model [14], the torques due to flexures are given by

$$T_i = -K_i\psi_i,\ i = 1, 2, 3, \text{or } 4. \tag{5}$$

Here, K_i represents the stiffness of the ith joint, and ψ_i is the angular change for the ith flexure, which is given by

$$\psi_i = (\theta_i - \theta_{i,0}),\ i = 1, 2, 3, \text{or } 4. \tag{6}$$

Here, θ_i is the joint angle, and $\theta_{i,0}$ is the neutral angle when the ith flexure is unstressed (assumed midway in the range for the joint angle). Note that this method of modeling flexure stiffnesses applies to large deflection cases which the flexures do indeed undergo. Comparisons of this model with more sophisticated finite element models indicate that it is sufficient for a first-order approximation [14].

Thus, the objective is to adjust the flexure stiffnesses for minimum input power (power supplied by the motor-gear box combination). As stated previously, only joints 3 and 4 are fabricated as flexure joints. The expressions for these angles are given as follows:

$$\psi_3 = (\theta_4 - \theta_{4,0}) - (\theta_3 - \theta_{3,0}),\ \psi_4 = (\theta_4 - \theta_{4,0}). \tag{7}$$

Note that the included angle at joint 3 depends on the movement of both the coupler and rocker links.

C. Theoretically Predicted Trends

As mentioned previously, only joints 3 and 4 are flexure joints; therefore, we consider the case when both these joints have nonzero but equal revolute stiffnesses. The results of the analysis described in the following show that the input power decreases as the stiffness is increased up to a point and then starts increasing again. We choose to consider the case of equal stiffnesses in both joints for the sake of convenience. Different flexure revolute stiffnesses are possible but not considered here.

The power analysis procedure is to sum the powers (torque times the appropriate angular velocity) due to all the torques and set it equal to zero and solve for the input torque. Since $\omega_w = \omega_4$, the resulting power balance (see Fig. 2) is given as follows:

$$T_{in}\omega_2 = (T_{w,a} + T_{w,i} + T_4)\omega_4 + T_3\omega_3. \tag{8}$$

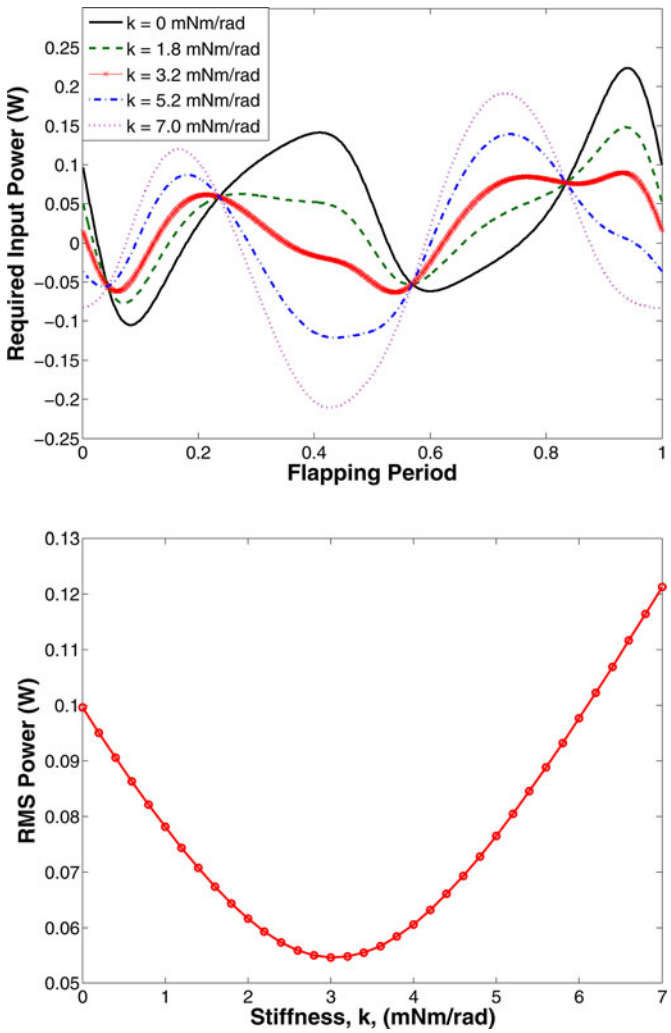

Fig. 3. (Top) Required input power to the transmission for five different flexure stiffness cases over one flapping period when flapping at 18 Hz. (Bottom) Trend of the RMS power to the transmission as the stiffness k is varied.

$T_{w,i}$ was calculated as given in (1) and $T_{w,a}$ was determined using (3) and (4) assuming the density of air of 1.22 kg/m^3 and a C_D of 2. The torques exerted by the flexure joints were calculated using (5) and (7). The parameters characterizing the wing were determined using an equivalent rectangular wing to the fabricated wing shown in Fig. 1, resulting in a mass of 143 mg (combination of the wing mass and half the mass of the linkages), a wing length of 62 mm, and an average chord of 37 mm. The angular velocities and accelerations were determined by solving the appropriate four-bar equations with the following link lengths: 1.41-mm crank, 8.41-mm coupler, 2.0-mm rocker, and 8.53-mm ground. The input crank velocity was taken to be $2\pi f_0$ and constant with f_0 representing the frequency. The value of f_0 was estimated as 18 Hz from encoder data taken with the wings flapping in our desired operating range. We should emphasize that the resulting input power is the mechanical input power to the transmission and not the electrical input power to the motor. Estimating the input power to the motor would require motor and gear efficiency data that are currently unavailable.

Fig. 3 plots the required input power to the transmission

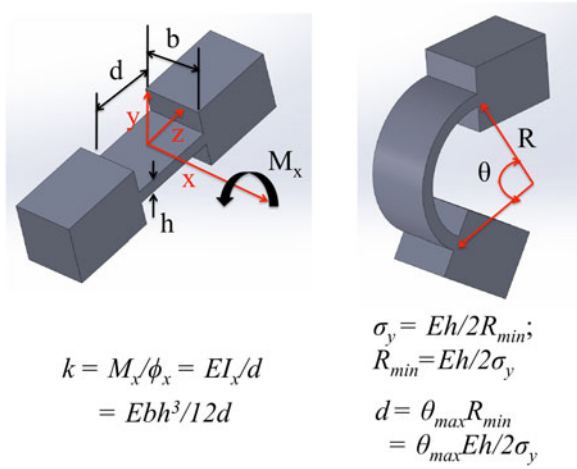

Fig. 4. Typical beam-type flexure and the basis of the two main flexure design considerations.

with no stiffness, 1.8 mN·m/rad stiffness, 3.2 mN·m/rad stiffness (that minimizes RMS power), 5.2 mN·m/rad stiffness, and 7.0 mN·m/rad stiffness. This optimal RMS stiffness of 3.2 mN·m/rad resulted in an overall savings in the RMS power value of about 45% over the no-stiffness case. It should be noted, however, that to make the model tractable, the joints are modeled as ideal torsional springs with no damping losses and massless. Motor and gearbox losses, as well as frictional losses, are also neglected. Therefore, we do not expect to see these kinds of power savings in our experiments. The theoretical trends are mainly used to estimate the desired flexure stiffness, while the actual power savings will be measured experimentally.

III. Transmission and Flexure Design

As demonstrated previously, compliant flexure joints help reduce the mechanical input power through potential energy storage. They also provide additional advantages in terms of reduced cost and space requirements, significant weight savings, and reduced wear and lubrication requirements compared with traditional pin joints. Flexure joints, however, introduce design challenges for use in FWMAVÕs because of large deformations associated with large stroke amplitudes. In what follows, we will discuss flexure design issues, material selection, and fabrication procedures.

A. Flexure Design

Once a theoretically motivated flexure stiffness that minimizes the RMS input power is determined, it can be used to design the flexure joint. Design considerations for flexures have been studied extensively with detailed discussions found in [14], [18], and [19]. The main focus here, however, is on matching the revolute stiffness of the fabricated flexure with our desired flexure stiffness. Relationships based on elementary mechanics of materials that are commonly used in the preliminary design of flexures are shown in Fig. 4. For a beam-type flexure,

the revolute stiffness is given by

$$k = \frac{EI}{d} = \frac{Ebh^3}{12d}. \tag{9}$$

Here, E is Young's modulus of the flexure material, I is the moment of inertia, b is the flexure width, h is the flexure thickness, and d is the flexure length. (Again, see Fig. 4.) Once the material of the flexure (and hence Young's modulus) is chosen, then the flexure dimensions can be appropriately determined. Another constraint is determined by the material's yield strength σ_y and the maximum angle that the flexure will move through $\theta_{\max}$. In order not to exceed the material's yield strength, and, hence, risk fatigue or fracture, the flexure's length should equal or exceed the following length:

$$d = \frac{\theta_{\max} Eh}{2\sigma_y}. \tag{10}$$

The basis for this relationship is shown on the right side of Fig. 4.

Table I illustrates the implications of the material choice on the resulting flexure dimensions. Note that to match the desired stiffness with polyimide film, the film needs to be relatively thick (200 μm) to approach a reasonable width of approximately 7 mm, but then, the length requirement (3.8 mm) starts to interfere with the compactness of the overall mechanism. Stainless steel is not a viable option for similar reasons. In addition, the added weight of a steel flexure of required dimensions is excessive. Because of their abilities to undergo large deformations before tearing and their relatively low densities, rubbers or elastomers thus become the materials of choice. Note, however, that there are other secondary concerns when designing flexures, for example, the relationship of off-axis stiffness with the revolute stiffness and viscoelastic losses in the materials. While we leave these details to the background references, they did influence the final flexure design, as discussed in Section III-C.

To further explain our choice of rubber (as opposed to, say, steel) as the flexure material, we note that besides joining the links, the flexures do double duty as energy storing torsional springs. This means that the flexure that deforms to the smallest radius of curvature ($R_{\min}$) can potentially store the most energy. From a material standpoint, this implies that the flexure material with the largest yield strain (see Fig. 4) is the best choice. For rubber, this value is 1.32, and on the other end of the spectrum, the corresponding value is 0.001 for stainless steel. If, instead, we redesign the structure so that the energy is stored elsewhere (for instance, in discrete springs), the material of choice would be the one with the highest ratio of $\sigma_y^2/\rho E$ when weight matters, as is the case here. However, even in that case, elastomers still tend to fare better than metals due to the much higher density of metals with the only drawback being elastomers' high loss factors [20].

B. Layered Process for Transmission Fabrication

After we have chosen the material and dimensions for the flexure, we then need to incorporate these flexures into the fabrication of the overall transmission mechanism. Because of the inherent advantages that flexure-based mechanisms offer (e.g., no friction or backlash and easy miniaturization), much work has been done to establish fabrication techniques to produce parallel linkages that are flexure-based [21]–[24]. The most recent evolution, and the technique adapted here, uses precured sheets of carbon fiber (for the rigid parts), acrylic adhesive sheets (Dupont FR1500), and polyimide film (for the compliant parts, Dupont Kapton). Each layer is individually laser micromachined (therefore, the carbon fiber or adhesive is removed from places where the flexures should be). The polyimide layer is then sandwiched between adhesive layers with the carbon fiber layers on top and on the bottom. Precise alignment is achieved through the use of alignment holes and precision dowel pins, as shown in the top of Fig. 5. The whole layup is then placed under 690 kPa pressure and cured at 204 °C for 2 h.

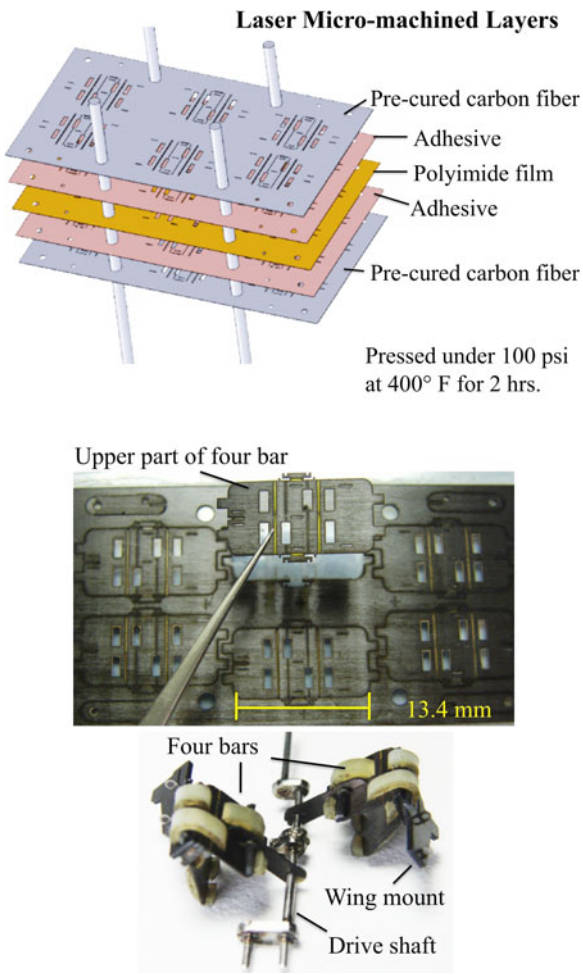

Fig. 5. (Top) Individual laser micromachined layers that are press cured together to form (middle) the composite structure. The rubber elements are woven into this structure, and it is folded up and assembled (with a wing mount added) to form (bottom) the four-bar transmission.

After the layers are cured together, the compound sheet is returned to the laser and the final outline cut is made. The structure is then released from the sheet (see the middle of Fig. 5), the rubber elements are added, and the structure is folded and assembled (see the bottom of Fig. 5). In this application, we weave the rubber elements and assemble by hand, but recent developments have demonstrated designs that assemble by simply

TABLE I
FLEXURE DIMENSIONS TO ACHIEVE DESIRED REVOLUTE STIFFNESS

Flexure Material	Desired Stiffness (Nm/rad)	Young's Modulus (GPa)	Yield Strength (MPa)	Thickness (mm)	Length $\theta_{max} = 60^\circ$ (mm)	Width (mm)	Weight (mg)
Kapton (Type 100 HN, Polyimide film)	0.0032	2.50	69.0	0.025 0.100 0.200	0.476 1.900 3.800	467.000 29.200 7.300	7.890
Stainless Steel Type 301	0.0032	193.00	205.0	0.050 0.100	24.700 49.400	39.300 9.830	390.000
Natural Latex Rubber	0.0032	0.02	26.5	0.508 0.635 1.020	0.201 0.252 0.404	2.950 1.890 0.731	0.274

opening up the structure with a single motion, as in a pop-up book [25].

C. Modified Cross-Flexure Development

As mentioned earlier, there are other concerns beyond achieving the desired revolute stiffness and adequate range of motion. These concerns include providing a well-defined axis of rotation and a good ratio of off-axis stiffness to revolute stiffness. For these two concerns, the relatively low Young's modulus of rubbers do not fare as well. For this reason, in addition to already having a well-established fabrication procedure described previously, we keep the relatively low-stiffness polyimide film flexures (in our designs, they have a stiffness of 0.15 mN·m/rad) and add rubber elements to provide the desired increased revolute stiffness. Because the polyimide film flexures are short (150 μm) and wide (7 mm), they provide a well-defined rotational axis with good off-axis stiffness. For example, the revolute stiffness about the y-axis, which is shown in Fig. 4, is given by $Ehb^3/12d$. Since, in this case, as high a stiffness as possible is desired, the considerable higher Young's modulus of polyimide compared with natural latex rubber (see Table I) increases this stiffness similarly. The same argument applies for other off-axis stiffnesses whose expressions can be found in [18].

In the first iterations of adding the elastic elements, we chose to do this by simply bonding a thicker silicone rubber (PDMS) layer to the existing carbon fiber and polyimide film structure. However, this is a challenging problem since rubbers typically resist bonding after they are cured or vulcanized. To overcome this problem, we have adapted methods previously used in microfluidics to bond PDMS to plastics [26], [27]. The method involves functionalizing the surfaces using silanes. Silanes typically have four groups attached to the silicon atom with one group having an inorganic reactivity and another having an organic reactivity making them ideal candidates to be used in the adhesion promotion of dissimilar materials, for instance, in the bonding between glass fibers and the epoxy matrix in glass fiber composites. We manipulate this use for bonding by exposing both materials to oxygen plasma to bring hydroxyl groups to the respective surfaces. Then, one material surface is exposed to an aqueous solution of silane (1–5% v/v) with an amino reactivity and the other to a solution (1–5% v/v) with an epoxy organic reactivity for 20 min. In both cases, the inorganic reactive group anchors to the hydroxyl groups brought to the surface, leaving one surface functionalized with the amino group and the other with the epoxy group. The surfaces are air dried, and when these surfaces are brought together, they bond readily due to the strong amino/epoxy connection. This method is desirable since it allows the linkages and these elastic flexure elements to be cured in their respective prescribed manners and then be bonded together at low temperatures, thus minimizing the effect of coefficient of thermal expansion mismatches. The results are shown in the top left part of Fig. 6.

While adequate bonding was achieved in static conditions, we did observe some delamination under dynamic loading. Rather than depending solely on bonding, we decided to provide mechanical constraints to hold the elastic elements in place. Additionally, since intuitively we expect the elastic elements to behave better when in tension rather than compression (buckling concerns, etc.), we incorporate a different configuration rather than the simple, beam-type flexures. Trease *et al.* give a comprehensive collection of different kinds of large displacement compliant joints [28]. The one of interest to us was the cross flexure (shown in the top right part of Fig. 6), which rates well for range of motion and low stress concentrations but poorly in axis drift and off-axis stiffness. By weaving two strips of the elastic elements (each 1.5 mm wide) on opposite sides of the traditional beam-type polyimide flexure (see the bottom part of Fig. 6), we have achieved a modified cross flexure design with a well-defined rotational axis, good off-axis stiffness, and with one elastic element always in tension regardless of which direction the flexure is bent. The polyimide flexure still experiences a stress concentration and, as such, is still subject to fatigue. However, in practice, we have found that the addition of the elastic elements increases the lifetime of the flexures. Systematic tests to characterize this increase in lifetime were not performed. However, we can state that the modified cross flexures with the thicker rubber strips routinely survived over 9000 cycles and, hence, in excess of the usual battery life for such FWMAVs. Because of the interchangeable nature of our design, these parts can be replaced upon failure, greatly extending the lifetime of such flyers.

Since the stiffnesses of springs in parallel add, if we subtract the contribution of the polyimide flexure from our desired stiffness and assume that the strip in tension is the one that contributes to the stiffness, we expect a latex rubber strip around 0.508 (20 mil) to 1.02 mm (40 mil) thick to approach a stiffness close to our target value, depending on the active length of the rubber strip as it crosses over the polyimide flexure.

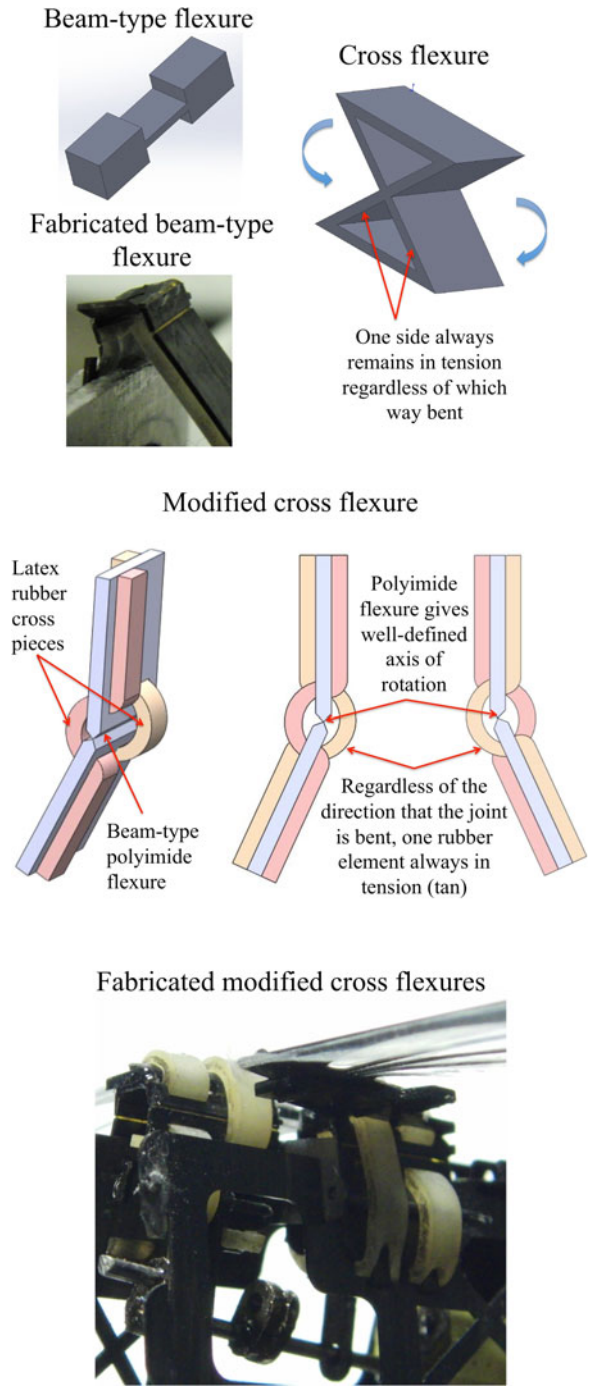

Fig. 6. Evolution of the design with the addition of rubber elastomer strips. The goal was to achieve the desired revolute flexure stiffness but still maintain a well-defined center of rotation and good off-axis stiffnesses that are not present in traditional cross flexures. The result was the modified cross flexure seen at the bottom of the figure.

Because our purpose here is to experimentally measure the effect that variation in flexure stiffness has on motor input power and resulting thrust, latex rubber was a logical choice of a representative elastomer due to its commercial availability in several film thicknesses. In addition, it has a higher modulus than PDMS (whose Young's modulus is around 750 kPa [29]), making the flexure dimensions more reasonable for this size scale.

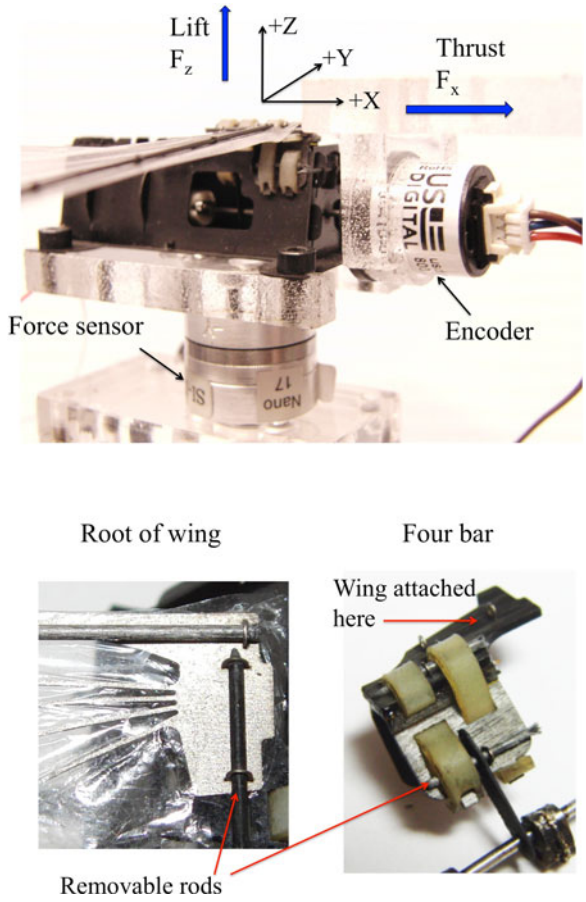

Fig. 7. Experimental test setup is shown. The body of the FWMAV is designed such that the wings and the upper part of the four-bar transmission can be exchanged for different sizes or flexure stiffnesses. The parts are attached (or detached) by removable carbon fiber rods.

However, on smaller scales, particularly where weaving in the elements might be difficult to do by hand, using PDMS and the previously described bonding techniques might become a viable option, particularly considering that PDMS is reported to have a low loss tangent [29].

IV. Experimental Test Setup

The experimental test configuration is shown in Fig. 7. The body of the FWMAV is secured to a six-axis force sensor (Nano17 Titanium, ATI Industrial Automation, with a 1.46-mN resolution) such that the thrust vector of the flyer is parallel to the x-axis of the force sensor (see Fig. 7 for convention). The motor driveshaft is extended outside the front of the body, and a magnetic encoder (MAE3, US Digital) is attached to record motor angular velocity and frequency. In addition to the forces and frequency, we also recorded the voltage and current being supplied to the motor. The data were recorded via a data acquisition board (NI PCI-6259, National Instruments Corporation, Austin, TX) and a LabVIEW (National Instruments) program.

The structure of the FWMAV has been designed in such a way that both the upper part of the four-bar mechanism (with the two flexure joints) and the wings can be conveniently replaced. This could involve replacing the transmission with a different flexure

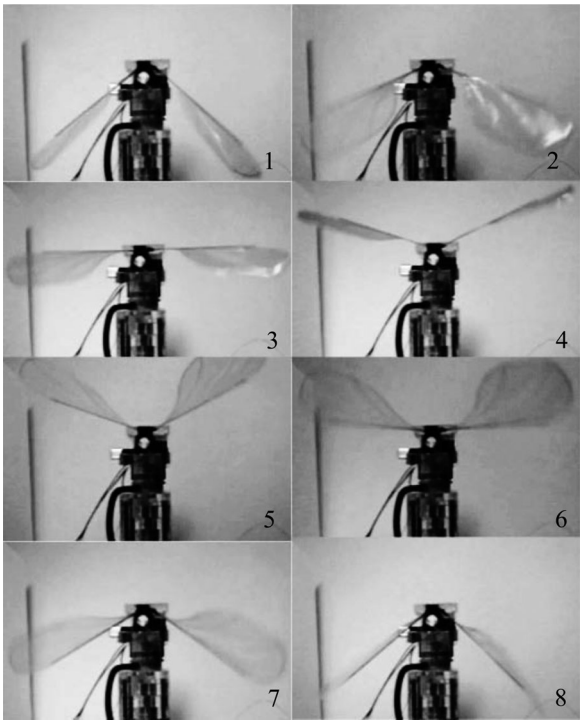

Fig. 8. Series of stills taken from high-speed video capturing the motion of the FWMAV when flapping at around 8.5 Hz with approximately 0.015 s lapse between frames.

stiffness or a different sized wing. In the tests conducted here, we chose to use natural latex rubber for the elastic elements and varied the strip's thicknesses. Optimization of the wing and wing rotation is not considered here; it is left for future work. Five different stiffness cases were tested: no latex rubber strips (polyimide flexures alone), 0.508 (20 mil), 0.635 (25 mil), 0.762 (30 mil), and 1.02 mm (40 mil) thick rubber strips. In all these tests with different flexures, the motor (GM15 25:1 6mm Planetary Gear Pager Motor, Solarbotics) and the wing, which is a titanium spar frame with a carbon fiber rod reinforcing the leading edge and laminated on both sides with 1.5-μm ultra polyester film, remained the same. Fig. 8 shows the flapping motion with approximately 3 V applied to the motor and the 0.635-mm flexure stiffness case. The series of stills is taken from high-speed video captured with a Casio EX-ZR100 at 420 frames/s.

V. Results and Discussion

For each of the flexure stiffness cases, power, frequency, and force data are recorded for at least 5–10 s interval at a 1 kHz sampling rate for different applied voltages. The data are then loaded into a MATLAB program where the average value at each measurement point for each of the measured properties is determined. Four separate trials like this are conducted and averaged. The results are shown in Figs. 9 and 10.

We first consider the power as the flapping frequency varies for each of the stiffness cases. The four-bar mechanism was designed to have as close to sinusoidal output as possible. Although due to the varying load from the wings on the motor, this

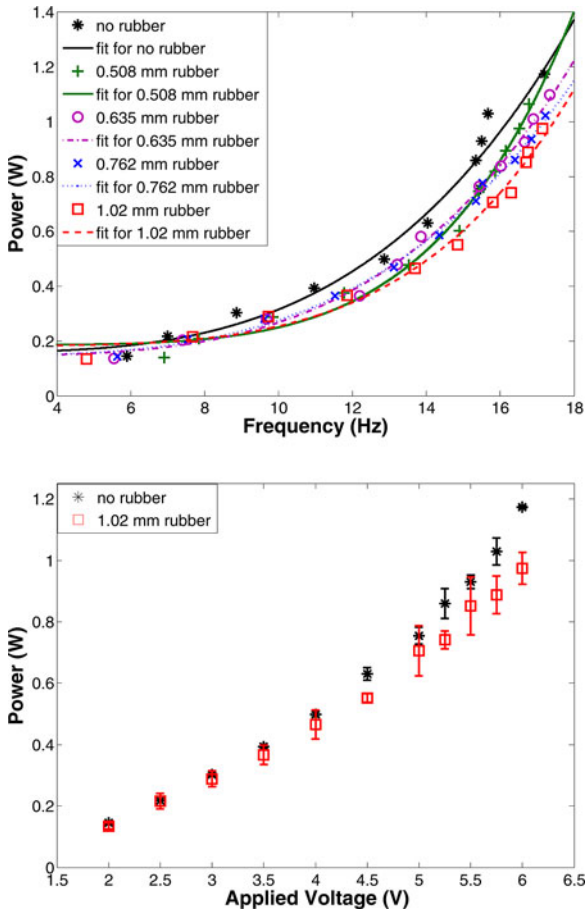

Fig. 9. (Top) Experimentally measured power supplied to the motor versus frequency shown for the five different stiffness cases. The greatest saving of power from the no-rubber case comes from the 1.02-mm case in the frequency range of interest (16–18 Hz). (Bottom) Error bars on the power data for the no-rubber and 1.02-mm rubber case as a function of the voltage applied to the motor control circuit.

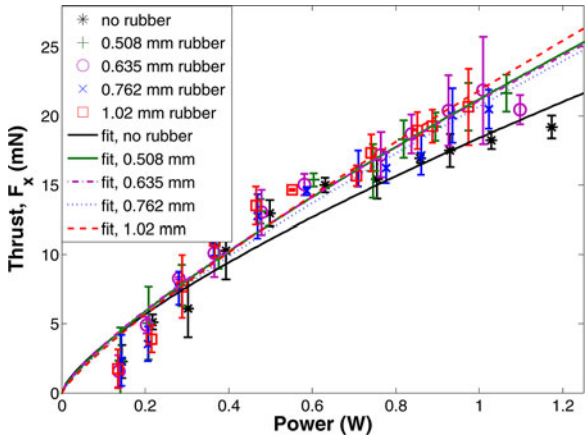

Fig. 10. Thrust production versus motor input power plotted for the five different stiffness cases along with the associated error bars for the thrust measurement. As can be seen, all the rubber cases produce 15–20% more thrust in the operating region of interest (1–1.25 W).

is not quite achieved in practice. However, for the purposes of determining how power should vary according to frequency, we assume it is fairly close. Thus, assuming a sinusoidally varying flapping angle of the form $\omega_w = \Omega_0 \sin(2\pi f_0 t)$, where Ω_0 is the amplitude, and f_0 is the frequency, it is easy to verify that ω_w and α_w, respectively, vary as f_0 and f_0^2. It then follows that the two major contributors to the input power, the inertial power and power due to aerodynamic damping [see (1) and (2)], both vary as f_0^3. As seen in Fig. 9, we therefore applied a power fit and then verified that the resulting fit was in the cubic range with the adjusted *R*-square values being 0.9596 for the no-rubber case, 0.9872 for the 0.508-mm case, 0.9946 for the 0.635-mm case, 0.9961 for the 0.762-mm case, and 0.9838 for the 1.02-mm case. From the results shown in Fig. 9, all the rubber cases generally use less power than the no-rubber case at the same frequency in the 8–18 Hz range. At the operating frequencies of interest here (16–18 Hz), however, the 1.02-mm-thick rubber shows the most power savings at generally 20% less power. Generally, it was seen that the introduction of the rubber flexures allowed for a small reduction in power and slight increase in frequency for a given applied voltage to the motor control circuit. In the bottom of Fig. 9, the reduction in power for each of the applied voltages is shown for the no-rubber and 1.02-mm rubber case along with the corresponding related error in the power measurement.

When we look at thrust production versus input power (see Fig. 10), we again see a similar gain for the rubber cases. In the operating region of 1–1.25 W (which corresponds to our desired frequency range of 16–18 Hz), the rubber cases produce 15–20% more thrust than the no-rubber case. This 3–4.5-mN gain in thrust is about twice the sensor resolution of 1.46 mN. According to classical Rankine–Froude theory [30], we expect the thrust to vary as input power raised to the 2/3 power, and such a power fit is applied in the figure. The adjusted *R*-squared values for the fits are 0.9377, 0.9692, 0.9547, 0.9473, and 0.9456 for the no-rubber to 1.02-mm case, respectively.

The measured power savings of 20% are considerably lower than the theoretical predictions of 45%. This difference highlights the fact that in the analysis in Section II, we are modeling the joints as ideal torsional springs (massless and no damping losses). In reality, this is not the case, and since we choose not to use traditional metal springs and instead incorporate this feature in the beam-type flexures, there are high losses associated with dissipated energy as heat when vibrated. In addition, the losses occurring in the motor and gearbox were neglected. As stated previously, we did not attempt to model these losses as much of the motor and gear efficiency data required to do this is currently unavailable for the motor used in this study. However, since the purpose of the study was to simply motivate that such power savings are indeed possible and provide a guide for appropriate flexure stiffnesses, such detailed modeling was not warranted here.

Finally, the advantages of incorporating this power-saving feature in the flexure joints results in other benefits such as overall weight savings, more integrated construction, and, hence, more robust structures. With the gain of 0.3 g of thrust with a less than 1% cost in weight (0.02 g) to the overall structure, the use of compliant elements in the flexures is justified.

VI. Conclusion

The aforementioned studies reveal that a given articulated transmission mechanism should incorporate a certain amount of spring stiffness to operate in a minimal power draw and maximal thrust production mode. With the limited weight and compactness requirements of centimeter-sized FWMAVs, certain materials, namely rubbers or elastomers, work better at providing this desired stiffness. Experimental data demonstrate that, given the same system (geared motor, fixed lengths for the transmission links, and same size wing), an optimal stiffness in the flexure joints (using latex rubber strips compared with no-rubber strips in the modified cross-flexure joints) produces similar thrust for around 20% less power. Similarly, when operating in the same power region (around 1 W), the rubber flexure cases produce around 15–20% more thrust than the no-rubber flexure case. This approximately 0.3 g added thrust is achieved with an only 0.02 g cost in weight (a less than 1% increase in weight assuming a total weight of around 3 g). While the power savings are less than what is predicted for ideal torsional springs, at least partially due to the high loss tangents of elastomers, the advantages of modest power savings and increased thrust at a very minimal cost in weight make their inclusion worthwhile.

VII. Future Work

Future work will involve the inclusion of an elastic hinge at the wing root for passive rotation and the use of the same experimental setup with interchangeable body parts to help optimize the thrust/lift production. We will also look at the effect of different wing sizes. Other potential studies might include the study of the use of different elastomeric materials and configurations. In nature, the material used for this purpose is resilin, which has an extremely high resilience (percentage of stored energy return between 90% and 97%) [31]. Exploration into different kinds of elastomers to minimize the loss tangent (or into attempts to produce artificial resilin materials) could potentially maximize these power savings.

Acknowledgment

The authors would like to thank P. Sreetharan, B. Finio, M. Smith, M. Karpelson, M. Kovac, J. Paik, H. Tanaka, M. Tolley, A. Baisch, K. Hoffman, K. Ma, Z. E. Teoh, and V. Sahai for useful discussions and assistance.

References

[1] R. M. Alexander, *Elastic Mechanisms in Animal Movement*. Cambridge, U.K.: Cambridge Univ. Press, 1998.

[2] G. A. Pratt and M. M. Williamson, "Elastic actuator for precise force control," U.S. Patent 5 650 704, 1997.

[3] D. W. Robinson, J. E. Pratt, D. J. Paluska, and G. A. Pratt, "Series elastic actuator development for a biomimetic walking robot," in *Proc. IEEE/ASME Int. Conf. Adv. Intell. Mechatron.*, Sep. 1999, pp. 561–568.

[4] M. Kovac, M. Fuchs, A. Guignard, J.-C. Zufferey, and D. Floreano, "A miniature 7g jumping robot," in *Proc. IEEE Int. Conf. Robot. Autom.*, May 2008, pp. 373–378.

[5] U. Scarfogliero, C. Stefanini, and P. Dario, "A bioinspired concept for high efficiency locomotion in micro robots: The jumping robot grillo," in *Proc. IEEE Int. Conf. Robot. Autom.*, May 2006, pp. 4037–4042.

[6] W. A. Churaman, A. P. Gerratt, and S. Bergbreiter, "First leaps toward jumping microrobots," in *Proc. IEEE/RSJ Int. Conf. Intell. Robot. Syst.*, Sep. 2011, pp. 1680–1686.
[7] J. P. Khatait, S. Mukherjee, and B. Seth, "Compliant design for flapping mechanism: A minimum torque approach," *Mech. Mach. Theory*, vol. 41, pp. 3–16, 2006.
[8] T. Tantanawat and S. Kota, "Design of compliant mechanisms for minimizing input power in dynamic applications," presented at the ASME Int. Des. Eng. Tech. Conf. Comput. Inf. Eng. Conf., Philadelphia, PA, Sep. 2006.
[9] S. S. Baek, K. Y. Ma, and R. S. Fearing, "Efficient resonant drive of flapping-wing robots," in *Proc. IEEE/RSJ Int. Conf. Intell. Robot. Syst.*, Oct. 2009, pp. 2854–2860.
[10] R. Madangopal, Z. A. Khan, and S. K. Agrawal, "Biologically inspired design of small flapping wing air vehicles using four-bar mechanisms and quasi-steady aerodynamics," *J. Mech. Des.*, vol. 127, pp. 809–816, 2005.
[11] Z. A. Khan and S. K. Agrawal, "Study of biologically inspired flapping mechanisms for micro air vehicles," *AIAA J.*, vol. 49, no. 7, pp. 1354–1365, 2011.
[12] W. Bejgerowski, A. Ananthanarayanan, D. Mueller, and S. Gupta, "Integrated product and process design for a flapping wing drive-mechanism," *ASME J. Mech. Des.*, vol. 131, no. 6, pp. 061006-1–061006-9, 2009.
[13] R. J. Wood, J. P. Whitney, and B. M. Finio, *Mechanics and Actuation for Flapping-Wing Robotic Insects*. New York: Wiley, 2011, ch. 12, pp. 4393–4406.
[14] L. L. Howell, *Compliant Mechanisms*. New York: Wiley-IEEE, 2001.
[15] C. P. Ellington, "The aerodynamics of hovering insect flight—I: The quasi-steady analysis," *Philosph. Trans. Roy. Soc. London Series B, Biol. Sci.*, vol. 305, pp. 1–15, 1984.
[16] R. L. Harmon, "Aerodynamic modeling of a flapping membrane wing using motion tracking experiments," M.S. thesis, Dept. Aerosp. Eng., Univ. Maryland, College Park, 2008.
[17] P. Nikravesh, *Computer-Aided Analysis of Mechanical Systems*. Englewood Cliffs, NJ: Prentice–Hall, 1988.
[18] M. Goldfarb and J. E. Speich, "A well-behaved revolute flexure joint for compliant mechanism design," *J. Mech. Des.*, vol. 121, pp. 424–429, 1999.
[19] S. Avadhanula and R. S. Fearing, "Flexure design rules for carbon fiber microrobotic mechanisms," in *Proc. IEEE Int. Conf. Robot. Autom.*, Apr. 2005, pp. 1579–1584.
[20] M. F. Ashby, *Materials Selection in Mechanical Design*. New York: Pergamon, 1992.
[21] E. Shimada, J. Thompson, J. Yan, R. J. Wood, and R. S. Fearing, "Prototyping millirobots using dexterous microassembly and folding," in *Proc. Symp. Microrobot., ASME Int. Mech. Eng. Congr. Expo.*, Nov. 5–10, 2000, pp. 933–940.
[22] R. J. Wood, S. Avadhanula, and R. S. Fearing, "Microrobotics using composite materials: The micromechanical flying insect thorax," in *Proc. IEEE Int. Conf. Robot. Autom.*, Sep. 2003, vol. 2, pp. 1842–1849.
[23] R. Sahai, E. Steltz, and R. S. Fearing, "Carbon fiber components with integrated wiring for millirobot prototyping," in *Proc. IEEE Int. Conf. Robot. Autom.*, Apr. 2005, pp. 1258–1263.
[24] R. Wood, S. Avadhanula, R. Sahai, E. Steltz, and R. Fearing, "Microrobot design using fiber reinforced composites," *J. Mech. Des.*, vol. 130, no. 5, pp. 052304-1–052304-11, May 2008.
[25] J. P. Whitney, P. S. Sreetharan, K. Y. Ma, and R. J. Wood, "Pop-up book MEMS," *J. Micromech. Microeng.*, vol. 21, no. 11, pp. 115021-1–115021-7, Nov. 2011.
[26] M.-E. Vlachopoulou, A. Tserepi, P. Pavli, P. Argitis, M. Sanopoulou, and K. Misiakos, "A low temperature surface modification assisted method for bonding plastic substrates," *J. Micromech. Microeng.*, vol. 19, pp. 015007-1–015007-6, 2009.
[27] L. Tang and N. Y. Lee, "A facile route for irreversible bonding of plastic-PDMS hybrid microdevices at room temperature," *Lab Chip*, vol. 10, pp. 1274–1280, 2010.
[28] B. P. Trease, Y.-M. Moon, and S. Kota, "Design of large-displacement compliant joints," *J. Mech. Des.*, vol. 127, pp. 788–798, Jul. 2005.
[29] J. C. Lotters, W. Olthuis, P. H. Veltink, and P. Bergveld, "The mechanical properties of the rubber elastic polymer polydimethylsiloxane for sensor applications," *J. Micromech. Microeng.*, vol. 7, pp. 145–147, 1997.
[30] S. Shkarayev and D. Silin, "Applications of actuator disk theory to membrane flapping wings," *AIAA J.*, vol. 48, no. 10, pp. 2227–2233, Oct. 2010.
[31] C. M. Elvin, A. G. Carr, M. G. Huson, J. M. Maxwell, R. D. Pearson, T. Vuocolo, N. E. Liyou, D. C. C. Wong, D. J. Merritt, and N. E. Dixon, "Synthesis and properties of crosslinked recombinant pro-resilin," *Nature*, vol. 437, pp. 999–1002, 2005.

Ranjana Sahai received the Ph.D. degree in mechanical engineering from the University of California, Berkeley, in 2006.

She was both a Marie Curie International Fellow and National Science Foundation Fellow with Scoula Superiore Sant'Anna and a Postdoctoral Fellow with the National Enterprise for NanoScience and NanoTechnology, Scoula Normale Superiore, Pisa, Italy. She is currently with the Harvard Microrobotics Laboratory, Harvard University, Cambridge, MA. Her research interests include the areas of micro/nano-fabrication, biologically inspired robotics, microrobotics, microfluidics, and crossover technologies between these areas.

Kevin C. Galloway received the Ph.D. degree in mechanical engineering from the University of Pennsylvania, Philadelphia, in 2010.

While he was with the University of Pennsylvania, he developed a composite tunable stiffness leg and experimentally investigated the role of passive variable compliance on a hexapedal running robot. He is currently a member of the Advanced Technology Team with the Wyss Institute for Biologically Inspired Engineering, Harvard University, Boston, MA. His research interests include applying knowledge of materials and prototyping techniques toward the development of bioinspired robots and medical devices.

Robert J. Wood (M'07) received both the Master's and Ph.D. degrees in electrical engineering from the University of California, Berkeley, in 2001 and 2004, respectively.

He is currently a Charles River Professor of engineering and applied sciences with the School of Engineering and Applied Sciences and the Wyss Institute for Biologically Inspired Engineering, Harvard University, Cambridge, MA. His research interests include the areas of microrobotics and bioinspired robotics.